

Empirical Force Field Derivation and Implementation for LiMO_2 (M: Ni, Mn, Co) Cathode Materials

N Tsebesebe, K Kgatwane, P Ngoepe, R Ledwaba

University of Limpopo, Materials Modelling Centre, Private Bag x1106, Sovenga, South Africa, 0727

Email: nkgaphe.tsebesebe@ul.ac.za

Abstract

Layered transition metal oxides LiMO_2 (M= Mn, Ni, Co), exhibit good electrochemical performances and are considered as the prototype materials in the first commercial lithium-ion products. However, their performance as individual cathode has shown drawbacks and ignited interest in transition metal doping to form highly efficient cathodes. Such interest has driven efforts towards development of interatomic potentials to help provide information pertinent to the fundamental aspects of the interaction between atoms and allow accurate modelling of structures. Developing force fields is a tedious process as such cost functions often feature several competing minima. This work aims to obtain interatomic interactions (Ni-Ni, Ni-O, Co-Co and Co-O) suitable for large scale simulations. The potentials are fitted from the cross-platform, streaming task runner (code-based) GULP. The procedure fits the ionic size (A_{ij}), dispersion parameter (C_{ij}), and the hardness of ions (ρ_{ij}), according to the Buckingham potentials. The fitted interactions produced structures with lattice constants with a difference of less than 1% in NiO and 8.75% in CoO in comparison to experimental data. Furthermore, they yielded elastic constants with a difference of 0.35% in NiO and 2.01% in CoO. The high temperature molecular dynamic calculations validated the potentials through the melting temperatures. The nanostructures and their radial distribution curves confirmed melting temperatures of 2250K and 2000K in NiO and CoO, respectively. These are in good agreement accord with the experimental melting temperatures of 2206K and 2228K for NiO and CoO, respectively. Moreover, the derived interatomic potential accurately simulates the structural properties and behavior of and LiCoO_2 . The findings of the current study will enable the implementation of these potentials into LiMO_2 (M: Ni, Co and Mn) structures for incorporation as dopants into the LiMnO_2 cathode material.

1. Introduction

The family of Li-ion battery cathodes defined as Li and Mn-rich NMC (or LMR-NMC) materials with the general stoichiometry $\text{Li}_{1-x}\text{Ni}_y\text{Co}_z\text{Mn}_w\text{O}_2$ ($0 < x < 0.2$; $w > 0.5$) have shown superior electrochemical and safety behaviour to the corresponding basic layered oxide Leifer et al. (2020). Furthermore, the Li-stoichiometric ternary transition metal oxide has the potential combinations of the rate performance of LiCoO_2 , the high capacity of LiNiO_2 , and the structural stabilization imparted by the presence of Mn. Thus, the major electrochemical activity is attributed to nickel, while cobalt also can play an active role only at high potentials. However, these materials may suffer from severe capacity and voltage fading upon cycling, which remains the primary barrier for their large-scale commercialization Rapulenyane et al. (2018). The layered-to-spinel transition is the leading cause for voltage fading. The capacity fading phenomenon, on the other hand, is related to several detrimental situations: blocking of Li^+ ions intercalation sites due to cationic disorder ($\text{Li}^+/\text{Ni}^{2+}$ exchange), and evolution of oxygen that reduces its involvement in red-ox activity during the reversible Li-ion intercalation processes Leifer et al. (2020). As such, doping LiMO_2 (M: Mn, Ni and Co) with transition metal and non-transition metal impurities is an effective way to optimize the electrochemical performance of the material (Aregai et al. 2019 and Hoang, 2017).

In condensed matter physics, the task of obtaining different structural properties of materials, simulated atomistically with many atoms is an almost prohibitive one, in terms of computational

effort with the current computer architectures. The use of atomistic simulation methods is becoming increasingly important in materials science Davis and González (2014). That is, molecular dynamic (MD) simulations require that the interatomic interactions (forces between atoms within a structure) are utilized at each step of performing a calculation particularly fitting interatomic potential. The interatomic potentials represent the potential energy of a collection of interacting atoms as a function of geometric variables, such as distance and angle. They provide the underpinning physical basis for molecular statics, molecular dynamics, and kinetic Monte Carlo simulations of radiation effects in materials Rapulenyane et al. (2018). Moreover, the nature of the interatomic bonding and atomic configuration is required before the calculations. However, producing classical interatomic potential as a substitute for the genuine quantum-mechanical interaction of the particles is highly desirable. The usual procedure is to fit some empirical interatomic potential function, depending on N parameters, requiring either agreement with certain macroscopic properties (structural, thermodynamical) or agreement between the predicted and observed energies and atomic forces to obtain ideal microstructures. As such, accurate force fields can provide a very good description of the structure and crystal properties of a material, including, e.g., thermal transport, mechanical deformation, defect formation energies, among others. Therefore, there is a strong need for the development of reliable interatomic potentials for layered materials, which would allow an exploration of scenarios that are computationally too expensive at the ab initio level Mora-Fonz D et al. (2020). In counter to that, the potential parameter sets describe

atomic interactions in crystal structures, particularly for utilization in MD calculations at high temperature to analyse if the dynamic motion of atoms is realistic in terms of the state transformation of the structures.

The interatomic potentials are fitted from typical primitive unit cells for the body-centred cubic (BCC) crystal structures for both NiO and CoO compounds. The BCC unit cell consists of a net total of two atoms (Ni and O or Co and O), the one in the centre (O) and eight eighths from the corners (Ni/Co). That is, each of the corner atoms is the corner of another cube, the corner atoms in each unit cell will be shared among eight unit cells. Moreover, the volume of each atom occupying the corner is shared between eight adjacent cells, as such the BCC structure has the equivalent volume of two atoms, at the central midpoint and the corner. Structures used in this work have the space group of Fm3M (225). In this work, the cross-platform, streaming task runner (code-based) GULP Gale (1997) is utilised to fit the Buckingham interatomic potentials. In the procedure, the ionic size (A_{ij}) is fitted together with dispersion parameter (C_{ij}), and the hardness of ions (ρ_{ij}), according to the Buckingham potentials. A simple two body potential function based on the Born model of ionic solids was used. Moreover, the derived force fields are utilised as input data on the high-temperature molecular dynamic (MD) simulation for validation purposes.

2. Methodology

The potentials were fitted from an empirical approach, to accurately reproduce the lattice parameters and elastic constants. The empirical potential fitting is an iteration process where the potential parameters are varied to minimize the discrepancies between the fitted results and experimental data. The process utilised the cross-platform, streaming task runner (code-based) GULP Gale (1997) script to perform the fitting. The script first allowed the ions to relax to their lowest energy configuration before the potential fitting. The fitting procedure used short-range potential form. The short-range potential was based on the Born and Mayer developed potential form:

$$\Phi_{ij} = Ae^{-\frac{ij}{\rho}} \quad (1)$$

where A and ρ are variable parameters. The strength of this effect was adjusted from the more flexible two-parameter exponential version of the Born-Mayer potential which resulted in Buckingham potential represented by Hirschfelder and Rice (1954):

$$\Phi_{ij} = Ae^{-\frac{ij}{\rho}} - \frac{C}{r_{ij}^6} \quad (2)$$

where A , ρ and C are varied parameters. Due to the short-range nature of the potentials, a cut-off value beyond which they are no longer evaluated is used. Moreover, to ensure the accuracy of the derived potentials, high-temperature molecular dynamics (MD) calculations were carried out on 20000 atoms nanostructures of NiO and CoO with the potentials as input to find the melting temperatures of the structures. Furthermore, the derived interatomic potentials were tested on 30000 atoms nanostructure of LiCoO₂.

The simulations were performed employing DL_POLY Forester and Smith (1996) code under microcanonical ensemble (NVE).

3. Results and Discussions

3.1 Interatomic Potential Fitting

The derived atomic interactions were between two atoms that are not directly bonded as a function of the interatomic distances. As such, the O²⁻ - O²⁻ interactions are the dominant interactions in oxides, and the transferability of these interactions was considered vital by taking the actual interactions from the molecular dynamics INPUT Tada et al. (2010). Hence, the short-range potentials parameters for Ni²⁺ - Ni²⁺, Ni²⁺ - O²⁻, Co²⁺ - O²⁻ and Co²⁺ - Co²⁺ pairs were derived. The derived Buckingham interatomic potentials are shown in table 1.

Table 1: The derived Buckingham interatomic potentials for NiO and CoO

| Ionic pair (ij) | A _{ij} (eV) | ρ _{ij} (Å) | C _{ij} (eV/Å ⁶) |
|-------------------------------------|----------------------|---------------------|--------------------------------------|
| Ni ²⁺ - Ni ²⁺ | 6393.86 | 0.27829 | 0.00 |
| O ²⁻ - O ²⁻ | 11782.88 | 0.23400 | 30.22 |
| Ni ²⁺ - O ²⁻ | 380400.00 | 0.15000 | 0.00 |
| Co ²⁺ - Co ²⁺ | 80948.00 | 0.200 | 10.00 |
| O ²⁻ - O ²⁻ | 11782.88 | 0.234 | 30.22 |
| Co ²⁺ - O ²⁻ | 58856.82 | 0.180 | 0.00 |

3.2 Validation of Interatomic potentials

3.2.1 Structural Properties

In general, oxides possess complex crystal structures on which theories of thermal conductivity have been based, resulting in hindering the applications of the theories to various oxides Hoang, (2017). This limits the understanding of the origin of the modest thermal conductivity Hoang, (2017). Hence, the accuracy of derived interatomic potentials was validated by comparing the experimental and calculated lattice parameters and volume as illustrated in table 2. This confirmed the value of A_{ij} and ρ_{ij} for O²⁻ - O²⁻, Ni²⁺ - Ni²⁺, Co²⁺ - Co²⁺, Ni²⁺ - O²⁻ and Co²⁺ - O²⁻. The exact comparison of the lattice parameters provided the same equilibrium interatomic distances in the NiO structure and 8.75%. On the other hand, the agreement between elastic constants of NiO provided an average percentage difference of 0.35%. Conversely, the CoO elastic constants produced an average percentage difference of 2.01%. The distinctive elastic constants provide smaller curvatures around the equilibrium bond lengths Tada et al. (2010). The stiffness of the materials was detected from the bulk moduli of the structure (Table 2), with a percentage difference of 16.85% NiO and 3.05% in CoO.

3.2.2 Molecular Dynamics

Accurate force fields provide an adequate description of the structure and crystal properties of a material. As such, the success of the interatomic potentials in large systems was demonstrated by performing the high-temperature molecular dynamics calculations with the derived potentials for NiO and CoO on 20 000 atomic

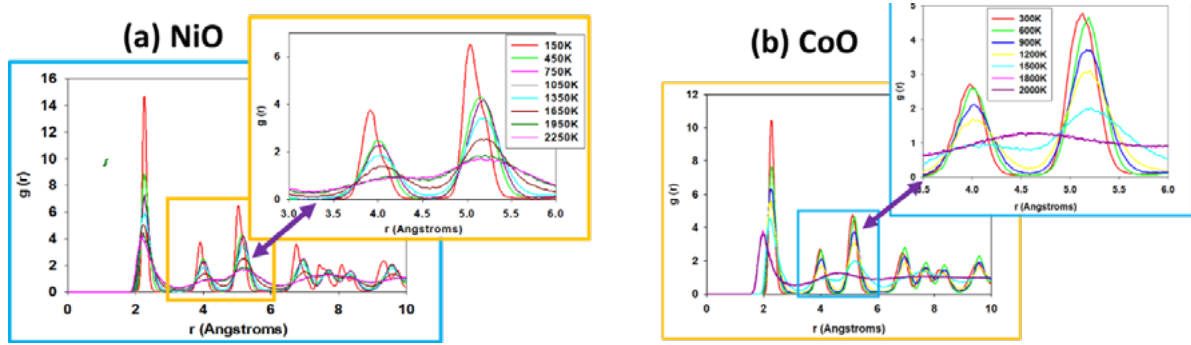


Figure 1: Radial distribution curves of (a) NiO and (b) CoO at various temperatures

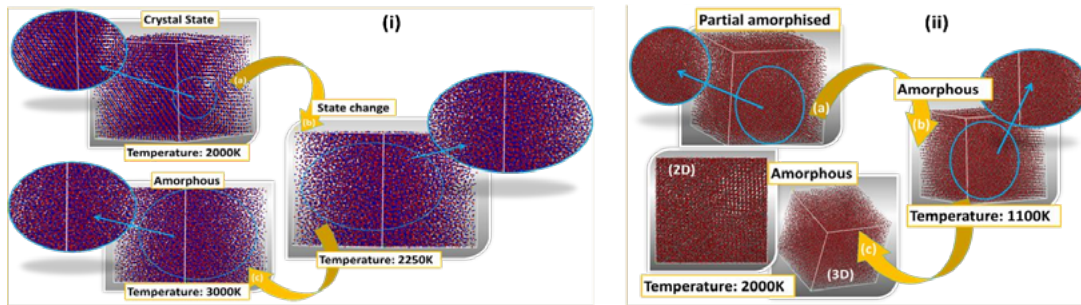


Figure 2: Molecular graphics representing phase transition in the melting region for (i) NiO and (ii) CoO

nanostructures, respectively. The nanostructures illustrated a phase change at 2250K and 2000K for NiO and CoO (table 3). Conversely, the probability of finding the nearest neighbouring atom when the NiO and CoO structures are heated to 2250K and 2000K respectively, is exceptionally low suggesting a phase transformation on the material (figure 1). Moreover, the nanostructures for NiO and CoO with generated interatomic potentials are depicted in figure 2 for further reference. Hence, NiO remains in a crystalline form from the temperature of 0K-2000K, figure 2 (a). The structure changes from the crystalline form into an amorphous state, when heated under temperature between 2250K and 2500K figure 2 (i and ii). Conversely, the CoO structure remains in the crystalline form when heated between 0K to 1000K shown in figure 2 (a). The transition from crystalline to amorphous state is present from 1100K to 2000K illustrated in figures 2 (a, b

and c). These are in good agreement accord with the experimental melting temperatures of 2206K and 2228K for CoO and NiO, respectively (table 3).

The 30000-atom LiCoO_2 orthorhombic nanostructure with RM space group further proved the accuracy of the derived interatomic potentials, from high-temperature molecular dynamics depicted in figure 4. The nanosphere maintains a crystalline state when subjected to temperature variation in the range of 0-1200K shown in figure 4 (a-c). As temperature is increased further, the structure transitions to an amorphous state above 1200K shown in the figure 4 (c, d and e). In addition, the RDF curves in figure 5 (a and b) shows maximum probability of finding nearest neighbor atom at the lowest temperature (400K to 1200K) suggesting phase change in the material. The probability and width of the curves decrease with increasing temperature, and the peaks becomes wider, as

Table 2: Comparisons of structural properties and elastic constants (GPa) of NiO and CoO

| | NiO | | CoO | |
|-------------------------|-------------------|-----------------------|-------------------|---------------------|
| | Calculated | Experimental | Calculated | Experimental |
| Lattice Parameters (Å) | $a = 4.42$ | $a = 4.42$ [11] | $a = 4.26$ | $a = 4.65$ [12] |
| Volume (Å^3) | 86.03 | 86.06 [11] | 100.57 | 77.31 [12] |
| Elastic constants (GPa) | $C_{11} = 344.65$ | $C_{11} = 342.7$ [13] | $C_{11} = 275.27$ | $C_{11} = 307$ [13] |
| | $C_{12} = 86.60$ | $C_{12} = 141.3$ [13] | $C_{12} = 188.26$ | $C_{12} = 183$ [13] |
| | $C_{44} = 86.60$ | $C_{44} = 41.2$ [13] | $C_{44} = 188.26$ | $C_{44} = 90$ [13] |
| Bulk Modulus (GPa) | 172.62 | 204.4 [13] | 217.26 | 224 [13] |

Table 3: Comparison of the melting temperature (K) for NiO and CoO

| | Calculated | Experimental | Calculated | Experimental |
|-------------------------|------------|--------------|------------|--------------|
| | NiO | NiO | CoO | CoO |
| Melting temperature (K) | 2250 | 2228 [14] | 2000 | 2206 [15] |

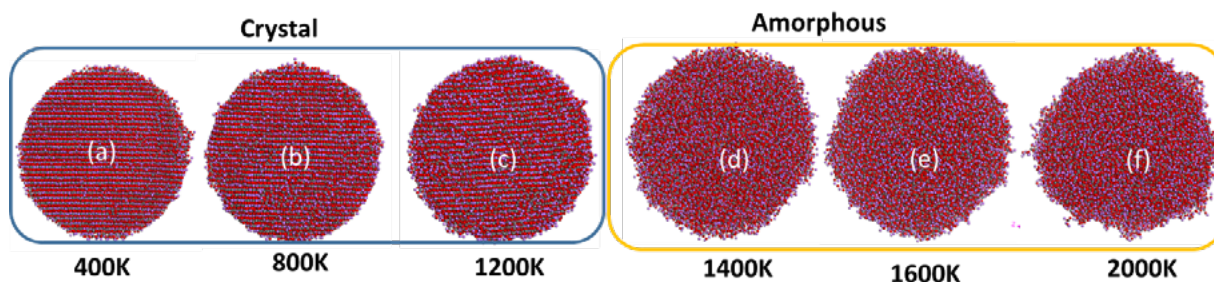


Figure 4 Molecular graphics representing phase transition from crystal (a-c) to amorphous (d-e)

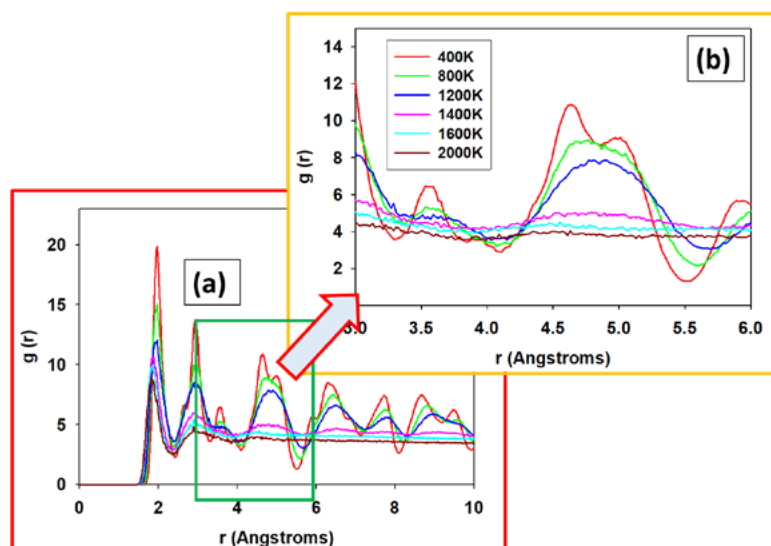


Figure 5 Radial distribution curves of LiCoO_2 at different temperature

shown in the figure 5(b). A complete phase transition, represented by a lower probability and a broader peak, is detected at 1400K, which confirms the melting point of the material. According to the experimental melting point of the material (1373 K) [16] Nakamura et al. (2018), the difference in melting point is 1.95%.

4. Conclusion

The Buckingham interatomic potentials were successfully fitted using a GULP code. The adjusted A , ρ and C parameters on the Buckingham formula led to the potentials match which can produce a structure with properties within 1 and 9 % of the experimental range. The fitted potentials produced the structural properties which compared relatively well with the experiment data. The molecular dynamics calculations performed from the potentials produced a structural phase change at temperatures in good agreement accord with the experimental melting temperatures. The radial distribution curves validated the structural phases from the probability of finding the nearest neighbouring atoms within the nanostructures. The derived interatomic potentials could be utilized to describe the structure and crystal properties of materials. Moreover, the derived interatomic potential accurately simulates the structural properties and behavior of LiCoO_2 material. That is, the findings of the current study will enable the implementation of these potentials into LiMO_2 (M : Ni, Co and Mn) structures for incorporation as dopants into the LiMnO_2 cathode material.

Acknowledgements

This research work has been performed using resources at the Materials Modelling Centre (MMC), University of Limpopo and the Centre for High-performance Computing (CHPC). This work was supported by the National Research Foundation.

References

- Leifer, N., Penki, T., Nanda, R., Grinblat, J., Luski, S., Aurbach, D. and Goobes, G., 2020. Linking structure to performance of $\text{Li}_{1.2}\text{Mn}_{0.54}\text{Ni}_{0.13}\text{Co}_{0.13}\text{O}_2$ (Li and Mn rich NMC) cathode materials synthesized by different methods. *Physical Chemistry Chemical Physics* 22, 9098-9109.
- Rapulenyane, N., Ferg, E. and Luo, H., 2018. High-performance $\text{Li}_{1.2}\text{Mn}_{0.6}\text{Ni}_{0.2}\text{O}_2$ cathode materials prepared through a facile one-pot co-precipitation process for lithium ion batteries. *Journal of Alloys and Compounds* 762, 272-281.
- Zong, H., Pilania, G., Ding, X., Ackland, G.J. and Lookman, T., 2018. Developing an interatomic potential for martensitic phase transformations in zirconium by machine learning. *Computational Materials* 4, 1-8503.
- Aregai, G.T., Babu, K.V., Babu, B.V., Rao, P.S. and Veeraiiah, V., 2019. Structural, electrical and electrochemical studies of copper substituted layered $\text{LiNi}_{1/3}\text{Co}_{1/3}\text{Mn}_{1/3}\text{O}_2$ cathode materials. *South African journal of chemical engineering* 27,43-52.
- González, D. and Davis, S., 2014. Fitting of interatomic potentials without forces: A parallel particle swarm optimization algorithm. *Computer Physics Communications* 185, 3090-3093.
- Mora-Fonz, D., Schön, J.C., Prehl, J., Woodley, S.M., Catlow, C.R.A., Shluger, A.L. and Sokol, A.A., 2020. Real and virtual polymorphism of titanium selenide with robust interatomic potentials. *Journal of Materials Chemistry A* 8, 14054-14061.
- Gale, J.D., 1997. GULP: A computer program for the symmetry-adapted simulation of solids. *Journal of the Chemical Society, Faraday Transactions* 93, 629-637.
- Rice, W.E. and Hirschfelder, J.O., 1954. Second virial coefficients of gases obeying a modified Buckingham (exp—six) potential. *The Journal of Chemical Physics* 22, 187-192.
- Smith, W. and Forester, T.R., 1996. DL POLY 2. 0: A general-purpose parallel molecular dynamics simulation package. *Journal of molecular graphics* 14, 136-141.
- Tada, M., Yoshiya, M. and Yasuda, H., 2010. Derivation of interatomic potentials from Ab-initio calculations for molecular dynamics simulations of Na_xCoO_2 . *Transactions of the Materials Research Society of Japan* 35, 205-208.
- Leineweber, A., Jacobs, H. and Hull, S., 2001. Ordering of nitrogen in nickel nitride Ni_3N determined by neutron diffraction. *Inorganic chemistry* 40, 5818-5822.
- Avalos, A., Zelaya, E. and Esquivel, M.R., 2021. A facile platform for the synthesis of metal–oxide composites. *Ceramics International* 47, 6972-6981.
- Uchida, N. and Saito, S., 1972. Elastic constants and acoustic absorption coefficients in MnO , CoO , and NiO single crystals at room temperature. *The Journal of the Acoustical Society of America* 51, 1602-1605.
- “Nickel(ii) oxide-wikipedia,” Wikipedia, [Online] Available: https://en.wikipedia.org/wiki/Nickel%28II%29_oxide. [Accessed 17 September 2021].
- “Cobalt(ii) oxide-wikipedia,” [Online]. Available: https://en.wikipedia.org/wiki/Cobalt%28II%29_oxide. [Accessed 17 September 2021].
- Nakamura, S., Maljuk, A., Maruyama, Y., Nagao, M., Watauchi, S., Hayashi, T., Anzai, Y., Furukawa, Y., Ling, C.D., Deng, G. and Avdeev, M., 2018. Growth of LiCoO_2 single crystals by the TSFZ method. *Crystal Growth & Design* 19, 415-420.